Brain Topography, Volume 18, Number 2, Winter 2005 (©2005)
DOI: 10.1007/s10548-005-0279-5

Integrated MEG and fMRI Model: Synthesis and Analysis

Abbas Babajani*, Mohammad-Hossein Nekooei*, and Hamid Soltanian-Zadeh*+

Summary: An integrated model for magnetoencephalography (MEG) and functional Magnetic Resonance Imaging (fMRI) is proposed. In the model, the neural activity is related to the Post Synaptic Potentials (PSPs) which is common link between MEG and fMRI. Each PSP is modeled by the direction and strength of its current flow which are treated as random variables. The overall neural activity in each voxel is used for equivalent current dipole in MEG and as input of extended Balloon model in fMRI. The proposed model shows the possibility of detecting activation by fMRI in a voxel while the voxel is silent for MEG and vice versa. Parameters of the model can illustrate situations like closed field due to non-pyramidal cells, canceling effect of inhibitory PSP on excitatory PSP, and effect of synchronicity. In addition, the model shows that the crosstalk from neural activities of the adjacent voxels in fMRI may result in the detection of activations in these voxels that contain no neural activities. The proposed model is instrumental in evaluating and comparing different analysis methods of MEG and fMRI. It is also useful in characterizing the upcoming combined methods for simultaneous analysis of MEG and fMRI.

Key words: Functional Magnetic Resonance Imaging (fMRI); Magnetoencephalography (MEG); Extended balloon model; Integrated model; Post Synaptic Potential (PSP).

Introduction

Magnetoencephalography (MEG) and electroencephalography (EEG) detect weak magnetic fields which can be generated by the flow of synchronized intracellular postsynaptic currents of pyramidal cells (Hämäläinen et al. 1993). Functional Magnetic Resonance Imaging (fMRI) signal reflects oxygen level of the blood and thus is called blood oxygen level dependent (BOLD) (Ogawa et al. 1992), which is a complex function of multiple physical variables like blood flow, blood volume and blood oxygenation that changes by neural activities (Buxton et al. 1998; Friston et al. 2000). The spatiotemporal resolution of these two techniques is different. MEG has good temporal resolution in the order of millisecond, but its spatial resolution is poor due to the ill-posedness of the inverse solution. On the other hand, fMRI has good spatial resolution in the order of millimeter but poor temporal resolution due to the limited rate of change in the hemodynamic response.

Since MEG and fMRI are different views of a common source (neural activity), their combined analysis should improve the overall spatiotemporal resolution of the results. Several methods have been introduced for MEG/fMRI combined analysis (Dale and Halgren 2001; Dale et. al 2000; Horwitz and Poeppel 2002; Korvenoja et. al 2001; Liu et. al 1998; Martinez-Montes et al. 2004) where sophisticated methods have been introduced to extract information as much as possible using a data-driven strategy (the authors refer to them as a top-down methods). Although the integrated MEG/fMRI methods aim at reaching the spatial resolution of fMRI and temporal resolution of MEG, some basic questions exist. For example, what are the differences between the spatiotemporal responses of the two methods and what are the conditions that cause these differences?

In Nunez and Silberstein (2000), the authors enumerated conditions in which there may be difference between spatiotemporal responses of fMRI and MEG. They imply that in a given neural activity with detectable BOLD signal, opposite polarizations of excitatory post synaptic potential (EPSP) and inhibitory post synaptic

* Control and Intelligent Processing Center of Excellence, Electrical and Computer Engineering Department, University of Tehran, Tehran, Iran.

+ Image Analysis Lab., Radiology Department, Henry Ford Health System, Detroit, MI, USA.

Accepted for publication: October 8, 2005.

This work was supported in part by the Research Council of the University of Tehran, Tehran, Iran. The authors would like to thank Dr. John Moran from the Neurology Department, Henry Ford Health System, Detroit, Michigan, USA for his helpful discussions and kind assistance.

Correspondence and reprint requests should be addressed to Hamid Soltanian-Zadeh, PhD, Radiology Image Analysis Lab., Henry Ford Health System, One Ford Place, 2F, Detroit, MI, 48202, USA.

Fax: (313) 874-4494

E-mail: hamids@rad.hfh.edu

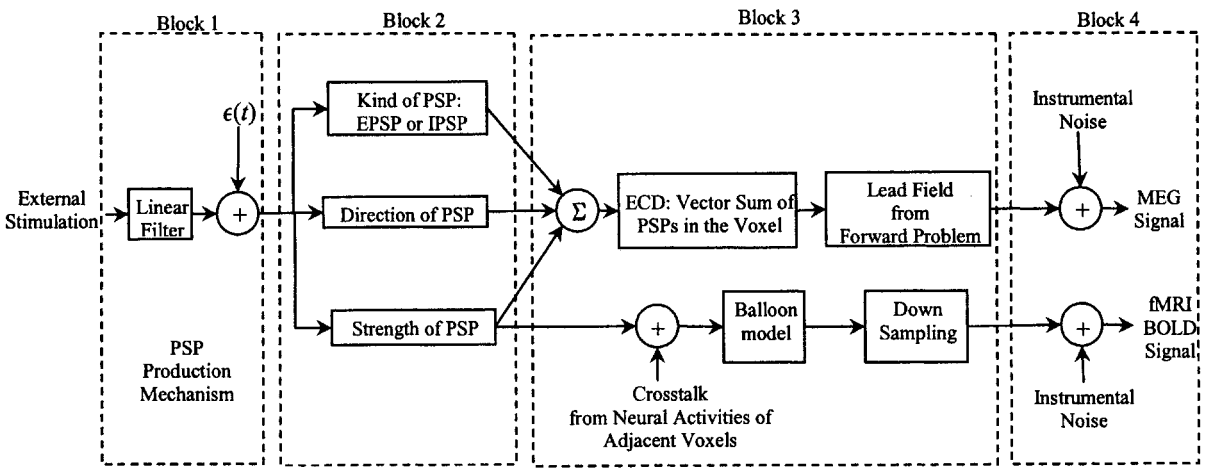

Figure 1. Schematic diagram for the proposed integrated MEG and fMRI model.

potential (IPSP) may cancel each other and thus no MEG signal is produced. In addition, activity in some cells like stellate cells whose dendritic tree is almost spherically symmetric produces BOLD signal but they are silent for MEG due to the fact that associated synaptic sources provide a spherically symmetric closed field structure. They also stated that the MEG signal can be large when a few percent of the neurons in each cortical column are "synchronously active" while the BOLD signal is weak.

For illustrating the relationship between MEG and fMRI, an integrated bottom-up model is required. If this model is based on physiological principles, different experimental conditions can be simulated by changing parameters of this model. In addition, it can be used for evaluating proposed methods for integrated MEG and fMRI analysis. The integrated model proposed by Riera and his colleagues (Riera et. al 2004; Riera et. al 2005) is one of the most recent works in this field. They introduced a two-dimensional autoregressive model with exogenous variables (ARx) to describe the interrelationships between synaptic activity and hemodynamics. Furthermore, they used a static nonlinear function to describe the electro-vascular coupling through a flow-inducing signal.

In this paper, we introduce a bottom-up integrated model based on the physiological principles (see figure 1). Post synaptic potentials (PSPs) and action potentials (APs) are two main indices for showing neural activities. It is assumed that both MEG and fMRI are only related to the PSPs (Baillet et al. 2001; Hämäläinen et al. 1993; Lauritzen and Gold 2003; Logothetis 2002, 2003, 2001). In the proposed model, PSPs are the main link between the MEG and fMRI. For a given external stimulus, a simple first order linear model represents the number of active PSPs at each time. Several parameters are introduced for the PSP whose variations in different neurons are modeled using random variables. Different aspects of EPSPs and IPSPs (like their directions and strengths) are used for producing MEG and BOLD signals.

In the fMRI part of the model, we introduce a relationship between the strength of the PSPs and neural activity which is used as input of the extended Balloon model (Friston et. al 2000) for producing the BOLD output. In the MEG part of the model, different spatial distributions and directions are considered for the EPSP and IPSP and equivalent current dipole (ECD) is calculated for each voxel using the vector sum of all active PSPs. A static Gaussian kernel is introduced for modeling the crosstalk from neural activities of the adjacent voxels in BOLD. Using computer simulations, we illustrate conditions where for a given neural activity it is possible to detect a BOLD signal but no MEG signal and vice versa.

It should be noted that whenever we write about the direction of the PSPs, it is scientifically more accurate to use PSCs (postsynaptic currents) instead of PSPs (postsynaptic potentials). However, since the direction of PSC is not important for fMRI and many of the MEG literature also use PSP instead of PSC, we use PSP throughout this paper.

Integrated Model

The proposed model relates the MEG and fMRI signals in an active voxel of the brain. The model is constructed based on the fact that PSPs are the main link between the two techniques. Since each voxel of the cortex contains a huge number of neurons and synapses whose activities are not deterministically known, we consider a stochastic model for PSPs whose parameters (like direction and strength) have a probability density function (pdf). The MEG signal is produced according to both direction and strength of the PSPs. The BOLD only de-

pends on the overall strengths of PSPs, which is the input of the extended Balloon model for producing the BOLD signal. An overview of the physiological principles that lead to the proposed integrated model is presented in the following subsection before introducing the model.

Neural Basis of MEG and fMRI

Pyramidal cells, inhibitory interneurons, and stellate cells are basic cell types in the neocortex where the first two constitute about 75-80% and 10-25% of all neurons, respectively (Buxhoeveden et al. 2002). MEG and fMRI signals reflect different aspects of the neural activity in these cells. The MEG signal is usually related to activation of the pyramidal cells. These cells are relatively large and their apical dendrites are parallel to each other and perpendicular to the cortical surface. Thus, the current dipoles of the PSPs add up. Dendrites of the stellate and interneuron cells occupy roughly spherical volumes and thus do not contribute significantly to the MEG signal. Activation in all neurons consumes energy thereby increasing regional cerebral blood flow (rCBF) and BOLD signal; there is no difference between the neurons in terms of the resulting BOLD signal in fMRI. In the integrated model, it is assumed that all neurons generate the fMRI signal but only the pyramidal cells generate the MEG signal.

Activity of each neuron starts with activities of its synapses that produce PSPs. The overall activities of the synapses may produce APs. PSPs and APs are two main indices for neural activities. In special cases, currents related to action potentials might contribute to the cortical MEG (and EEG) signals, e.g., high-frequency (about 600 Hz) somatosensory responses (Curio et al. 1994; Hashimoto et al. 1996). However, MEG signal seems to be largely due to the synaptic current flow (Baillet et al. 2001; Hämäläinen et al. 1993). On the other hand, based on several experimental results, it is reported that the BOLD signal is related to the PSPs and there is no correlation between the BOLD signal and the APs (Lauritzen and Gold 2003; Logothetis 2002, 2003, 2001).

There are some differences between the EPSP and IPSP from the MEG point of view. EPSP and IPSP have opposite polarizations and can cancel each other as considered in the proposed model. The spatial locations of the excitatory and inhibitory synapses are different. Excitatory synapses reach mainly the dendrite trees and inhibitory ones are attached to the soma and basal dendrites. Since neurons are small compared to their distances to the MEG sensors and we consider an ECD in each voxel, the location difference of EPSP and IPSP can be ignored. Another difference between EPSP and IPSP is spatial distribution of their directions. The basal dendritic tree of a neuron (with more inhibitory synapses) has approximately spherical symmetry while the apical dendritic tree (with more excitatory synapses) is approximately parallel (Liley and Wright 1994). The differences between the distributions of the directions of the EPSP and IPSP are considered in the proposed model.

In general, the relationships between the excitatory-inhibitory mechanisms and the hemodynamic-metabolic system need more investigation in the future (Attwell and Iadecola 2002). There is even doubt about the role of inhibition on increasing rCBF (Waldvogel et al. 2000). Tagamet and Horwitz (Tagamet and Horwitz 2001) introduce large-scale modeling to address the role of inhibition. Their simulations suggest that neuronal inhibition can raise rCBF if there is either low local excitatory recurrence or if the region is not otherwise driven by excitation. Conversely, inhibition can lower the observed values in situations with high recurrence or actively driven excitation.

Experimental study of Caesar and colleagues is one of the newest studies for investigating the role of inhibition in rCBF changes (Caesar et al. 2003). In several experiments, they stimulate the cerebellar climbing fibers (excitatory) and parallel fibers (inhibitory) alone and in combination, and simultaneously record the rCBF in the Purkinje cells. They report that stimulation of the excitatory climbing fibers (EPSP) or inhibitory parallel fibers (IPSP) increase the rCBF amplitude and there is no difference between EPSP and IPSP in this regards. Thus, they conclude that the EPSP and IPSP have similar effect on the BOLD signal.

However, it should be noted that neural inhibition decreases the overall activity and thus may reduce rCBF. In (Tagamet and Horwitz 2001) it is shown that for small local excitatory recurrence, inhibition causes rCBF to increase. In this situation, rCBF increase due to the added inhibitory activity is more than its decrease due to the reduction of the overall activity. Tagamet and Horwitz verify the other case of big local excitatory recurrence that inhibition decreases rCBF. In this case, the overall activity decreases due to the increased inhibitory activity. Thus, if inhibitory activity is considered independent of excitatory, it increases the rCBF and the decrease of the total rCBF is due to the reduction of the overall activity. EPSP and IPSP are independent in the proposed model. Since there is almost no difference between them for consuming energy, there is no difference between them from the fMRI point of view in the model.

It should be mentioned that the neuronal effect is different for postsynaptic and presynaptic inhibition. An IPSP is generated by postsynaptic inhibition but the presynaptic inhibition decreases the strength of the generated EPSP by involved excitatory synapse. Since the proposed model is based on different aspects of the EPSPs and IPSPs, our main focus is this paper is postsynaptic inhibition.

PSP Production Mechanism

Block 1 of figure 1 implements the relationship between the external stimulus and the number of active PSPs. The number of active PSPs at each time point is considered as the output of a linear system whose input is the external stimulus, similar to the linear model relating the external stimulus to the evoked transient in (Riera et al. 2004). The relationship between the number of active PSPs and strength of the stimulus may be nonlinear. However, for the sake of simplicity, we assume a linear model. This simplification does not have any influence on the relationship between MEG and BOLD signals in our model. The linear model is as follows.

$$\sum_{k=0}^{r} a_k \frac{d^k N(t)}{dt^k} = N_{ss} Stm(t - t_{af}) \tag{1}$$

where t_{af} is the delay due to different relay processes in the long afferent pathways. The first order linear model with $a_0 = 1$ and $a_1 = 50$ ms is used as the simplest linear model. For block design, $Stm(.)$ is the unit function and N_{ss} is the steady state value of $N(t)$. For event related design, $Stm(.)$ is the Dirac delta function and N_{ss}/a_1 is the peak value of $N(t)$. Physiological noise is modeled by $\in(t)$ in figure 1 and represents the number of active PSPs, which is not related to the external stimulus and is related to the spontaneous activity. It can be modeled as a Poisson process.

Constructing BOLD from PSPs

The first block of fMRI in the proposed model is "Crosstalk from Neural Activities of Adjacent Voxels" (see figure 1). Neural activities in a voxel change its blood flow and that of the neighboring voxels. In an experimental study on rats, it is reported that the diameter of local arterioles (at the stimulation site) increases 26% and local blood flow increases 55% while in an up stream region about 2 mm distant from the stimulation site, the diameter of arterioles increases 8.7% and blood flow increases 15% (Iadecola et al. 1997). In another experimental study on rats with electrical stimulation of the cerebellar parallel fibers, the local CBF at the stimulation site changes 55% while at sites with 4.5 mm horizontal and 1 mm vertical distance from the stimulation site, CBF changes 13% and 11%, respectively (Iadecola et al. 1996). Thus, the synaptic activities in a voxel can affect the CBF and resulting BOLD signal in adjacent voxels.

The Gaussian spatial smoothing kernel is used for modeling the spatial crosstalk of BOLD signal in the proposed model. We consider the effective synaptic activities as:

$$u_e(r;t) = G(r;o,\sigma) *** u(r;t); r = (x, y, z), \sigma = (\sigma_x, \sigma_y, \sigma_z) \tag{2}$$

where $u(r;t)$ is the synaptic activities in a voxel located at $r = (x,y,z)$, $G(r\ ;\ 0\ ,\ \sigma)$ is a 3D Gaussian kernel with zero mean and standard deviation σ and "$***$" shows 3D convolution. We use reported data from (Iadecola et al. 1996, 1997) and estimate σ by curve fitting of the reported data into a 3D Gaussian kernel. The estimated σ is 2.6 mm in the horizontal direction (axial slice) and 0.7 mm in the vertical direction (normal to axial slice) of the brain.

In the proposed model, extended Balloon model (Friston et al. 2000) is used as the main mechanism for relating PSPs (as the neural activity) to the BOLD. In the extended Balloon model, there is a set of nonlinear state space equations which relate the neural activity $u(t)$ to the BOLD. We will link PSPs to the extended Balloon model by introducing a relationship between PSPs and neural activity. In the simulations, the constant parameters of the extended Balloon model are the same as those used in (Friston et al. 2000).

The input to the extended Balloon model is the overall synaptic activities which are linearly related to the rCBF. We try to find a relationship between synaptic activity and PSPs. Each PSP consumes a small amount of energy and causes a small change in the blood flow. Thus, it is logical to consider synaptic activity (as input of the extended Balloon model) proportional to the total consumed energy by the PSPs. We need to solve the Hodgkin-Huxley (H-H) equation for computing the voltage, current, and energy of PSP. The PSP's voltage is modeled by multiplying a constant peak value ΔV and a normalized waveform $\varphi(t)$ (Almeida and Stetter 2002; Larkum et al. 1998):

$$\varphi(t) = \frac{te^{-\frac{(t-\tau_{PSP})}{\tau_{PSP}}}}{\tau_{PSP}} \tag{3}$$

$$V(t) = \Delta V \varphi(t) \tag{4}$$

where τ_{PSP} is time constant of $\varphi(t)$ and is considered as a random variable with truncated Gaussian distribution $\tau_{PSP} \sim TN(2,1;0,\infty)$ ms according to the data reported in (De Schutter 1998). The truncated Gaussian variable denoted by $x \sim TN(\mu, \sigma; a,b)$ is a variable whose probability for $x<a$ or $x>b$ is zero and its pdf is like the Gaussian distribution (except a scalar normalization) in the interval $x \in [a,b]$ with mean μ and standard deviation σ.

The consumed energy by PSP is found by:

$$E = \int_0^{\infty} V(t).I(t)dt \tag{5}$$

where $I(t)$ is PSC. For simplicity, we use a constant value for $I(t)$ and according to equations 3-5 get:

$$E = I\tau_{PSP}\Delta V \tag{6}$$

If $N(t)$ PSPs fire at time t, the consumed energy for each of them is represented by equation 6. The neural activity should be proportional to the sum of the consumed energy. Therefore, the following equation relates the synaptic activity (or neural activity) $u(t)$ to the parameters of the PSPs:

$$\begin{cases} E = \sum_{k=1}^{N(t)} E_k = \sum_{k=1}^{N(t)} I\tau_{PSP}^k \Delta V_k \propto \sum_{k=1}^{N(t)} \tau_{PSP}^k \Delta V_k \\ u(t) \propto \sum_{k=1}^{N(t)} \tau_{PSP}^k \Delta V_k \end{cases} \tag{7}$$

Activation of both pyramidal and non-pyramidal cells affects the BOLD signal, but the MEG signal is usually affected by the activation of the pyramidal cells. In each cortical area, the ratio of pyramidal to non-pyramidal cells is almost constant (4 pyramidal cells for each non-pyramidal cell). Thus, it can be assumed that the ratio of number of active PSPs of pyramidal to non-pyramidal cells is almost constant during the stimulus. By this assumption, $N(t)$ in equation 7 can represent the number of active PSPs of the pyramidal cells and right hand side of equation 7 is multiplied by a constant bigger than 1 and therefore the proportional form of equation 7 does not change. Another assumption in the proposed model is that the ratio of IPSP to EPSP numbers is constant during the stimulus. This can be justified by the fact that the ratio of inhibitory to excitatory synapses is fixed in each cortical area.

Constructing MEG Signal from PSPs

From a distance, the PSP looks like a current dipole oriented along the dendrite. Approximately, the current dipole due to PSP is (Hämäläinen et al. 1993):

$$\vec{q} = \frac{\pi}{4} d^2 \sigma_{in} \Delta V \cdot \vec{n} \tag{8}$$

$$\vec{q} = \beta \Delta V \cdot \vec{n} \quad , \quad \beta = \frac{\pi}{4} d^2 \sigma_{in} \tag{9}$$

where d is the diameter of the dendrite, σ_{in} is the intracellular conductivity per unit length, ΔV is change of voltage during PSP and $\vec{n}$ is unit vector which shows current dipole orientation along the dendrite. We consider the direction of current dipoles (of PSP) as a random variable for modeling different kinds of dendrite tree structures.

We define "reference vector" as a vector that is perpendicular to the cortical surface in each voxel. For the sake of simplicity, we assume cylindrical symmetry around the direction of the reference vector and consider only one parameter for modeling the angle between the reference vector and direction of each current dipole in our model. This angle in our model is θ which is considered as a truncated Gaussian random variable whose pdf is $f_\Theta(\theta)$.

$$\begin{cases} f_\Theta(\theta) = \dfrac{e^{\frac{-\theta^2}{2\sigma^2}}}{k} \\ \sigma_T^2 = \sigma^2\left(1 - \dfrac{2\pi\sigma^2}{k} e^{\frac{-\pi^2}{2\sigma^2}}\right) \end{cases} ; k = \sqrt{2\pi}\,\sigma\, erf\left(\frac{\pi}{\sqrt{2}\sigma}\right), -\pi < \theta \le \pi \tag{10}$$

where $erf(.)$ is the error function and σ is the standard deviation of θ whose pdf is considered as a Gaussian. σ_T is the standard deviation of the truncated θ whose pdf, $f_\Theta(\theta)$, is a truncated Gaussian. σ can get any positive value. As illustrated in figure 2, the pdf of θ tends to concentrate around zero when $\sigma \to 0$. The pdf of θ tends to the uniform distribution when $\sigma \to \infty$. The uniform distribution ($-\pi < \theta \le \pi$) is chosen for the pdf of θ in voxels that are not on the cortical surface. Thus, direction of the reference vector is not important in these voxels because directions of PSPs are uniformly distributed between -π and π.

Most of the excitatory synapses come from the apical dendrites that are parallel and perpendicular to the cortical surface. Thus, θ for EPSP has a distribution concentrated around the reference vector, i.e., the value of σ in equation 10 is small for EPSPs. A portion of the IPSPs comes directly to the soma which has the same direction as the trunk of the apical dendrites, therefore the value of σ is small for these IPSPs. However, the inhibitory synapses coming from basal dendrites have almost spherical spatial distribution, i.e., the pdf of θ for these IPSPs tends to a uniform distribution, which can be considered as a Gaussian with a large σ. Thus, the average value of σ for IPSPs is larger than its average for the EPSPs. Larger diameter of soma compared with dendrites produces different spatial distribution of the current flow after firing a PSP. Spatial distribution of the current flow after firing a PSP is mainly considered in the volume current which for the sake of simplicity is ignored in the proposed model because we consider spherically symmetric head model.

The current dipole q in equation 9 is projected onto two vectors, first vector (q_p) is parallel to the reference vector with the value of $q\cos(\theta)$ and the second vector (q_n) is orthogonal to the reference vector with the value of $q\sin(\theta)$. $E[q_n]$ is zero (according to odd property of $sin(.)$ and even property of $f_\Theta(\theta)$ in equation 10). Thus, for the

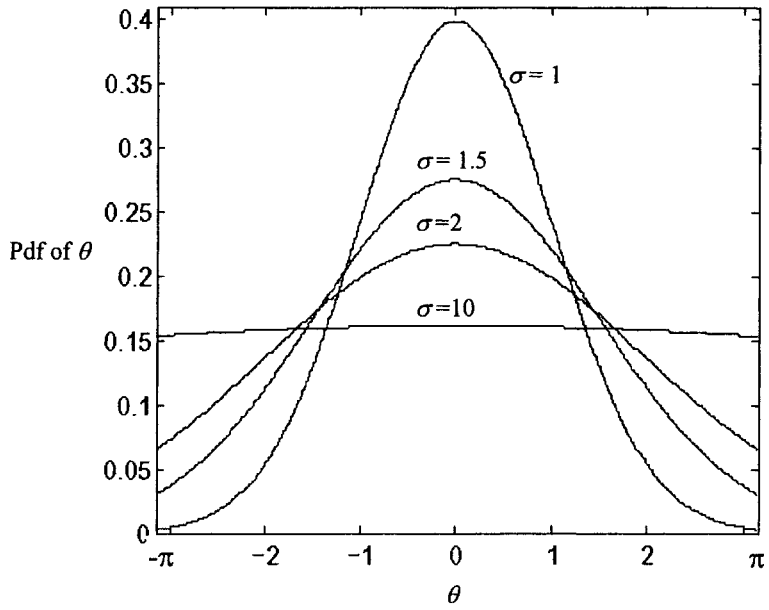

Figure 2. The pdf of θ (angle between current dipole and reference vector) according to equation 10 for 4 values of σ.

MEG sensors, q_n acts as noise without any correlations with the stimulation. On the other hands, $E[q_p]$ is nonzero and can be sensed by the MEG sensors as a signal. When $\sigma \to \infty$ in equation 10, distribution of θ tends to uniform distribution and then $E[q_p] \to 0$. It should be noted that the direction and moment of each current dipole (produced by a PSP) is modeled by several random variables in our model. To qualitatively verify the effect of these random variables on the MEG signal, we use $E[q]$ instead of q to evaluate the overall effect of these random variables.

If N PSPs of the pyramidal cells fire at time t, then the ECD from the sum of their activities according to equation 9 is:

$$\vec{q}(t) = \sum_{k=1}^{N} w_k \beta_k \Delta V_k \varphi_k(t) \cdot \vec{n}_k \tag{11}$$

where w_k is +1 for EPSP and -1 for IPSP, ΔV_k shows peak value of PSP, β_k is a coefficient according to equation 9 that models parameters of the kth synapse and its neighboring dendrite, and $\varphi_k(t)$ is unitary peak waveform for the kth PSP at time t according to equation 3. For modeling different kinds of synapses, we consider β_k and ΔV_k as random variables by using truncated Gaussian and uniform distributions. The uniform distribution variable denoted by $x \sim uniform(a,b)$ is a random variable whose probability is constant in the interval $[a,b]$ and zero outside of this interval. We assume ΔV_k as a truncated Gaussian distribution ($\Delta V_k \sim TN(10, 5; 0, \infty)$ mV) (De Schutter 1998) and β_k according to equation 9 as a function of two random variables ($d \sim uniform(0.1,2)$ μm and $\sigma_{in} \sim uniform(0.1,2)\ \Omega^{-1}m^{-1}$), based on the typical values of d =1 μm and σ_{in} =1 $\Omega^{-1}m^{-1}$ (Hämäläinen et al. 1993).

The number of pyramidal PSPs in a voxel that starts to fire at time t is denoted by $N(t)$. We sample $N(t)$ every millisecond in the simulations. The ECD in this voxel is derived from equation 11:

$$\vec{Q}(t) = \sum_{d=0}^{D} \sum_{k=1}^{N(t-d)} w_k \beta_k \Delta V_k \varphi_k(t+d) \cdot \vec{n}_k \tag{12}$$

where $\varphi_k(t+d)$ is the waveform of the kth PSP whose activation started at the previous d sampling times and D is the maximum duration of PSP which we set approximately D = 30 ms according to the maximum value of τ_{PSP} in equation 3. The projections of $\vec{Q}(t)$ onto two normal vectors can be found as:

$$\begin{cases} \vec{Q}(t) = \left[\sum_{d=0}^{D} \sum_{k=1}^{N(t-d)} w_k \beta_k \Delta V_k \varphi_k(t+d) \cos(\theta_k) \right] \cdot \vec{n}_p + \\ \left[\sum_{d=0}^{D} \sum_{k=1}^{N(t-d)} w_k \beta_k \Delta V_k \varphi_k(t+d) \sin(\theta_k) \right] \cdot \vec{n}_n \\ \vec{Q}(t) = Q_p(t)\vec{n}_p + Q_n(t)\vec{n}_n \end{cases} \tag{13}$$

where n_p is the unit vector parallel to the reference vector and n_n is the unit vector orthogonal to it.

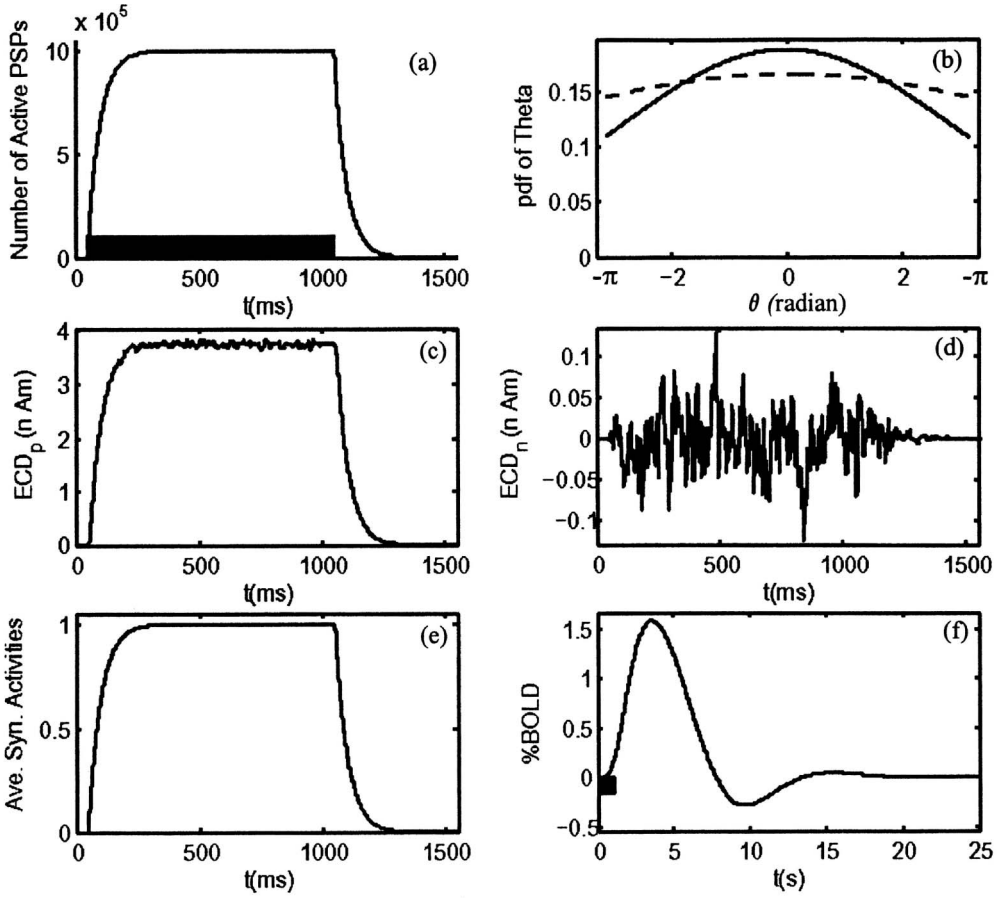

Figure 3. Illustration of the capability of the proposed model to generate both MEG and fMRI signals. The small black rectangle shows the duration of stimulation. (a) Number of active synapses according to equation 1 with a_0 =1, a_1=50 ms. (b) pdf of θ where θ is the angle between PSP dipole and direction perpendicular to the cortical surface. Solid and dashed lines represent EPSP and IPSP, respectively. (c) Projected ECD in the direction perpendicular to the cortical surface, $Q_p(t)$ in equation 13. (d) Projected ECD in the direction tangent to the cortical surface, $Q_n(t)$ in equation 13. (e) Average synaptic activity according to equation 7. (f) BOLD output with u/u_{max} = 0.2 and $u(t)$ as input neural activity from (e).

The "Lead Field from Forward Problem" is the final part of the MEG modeling in figure 1. Electrical potential and magnetic field, produced by activation in some voxels, can be computed by quasi-static approximation of Maxwell equations (Baillet et al. 2001). After choosing a head model (spherical approximation or realistic head model), the following matrix equation relates the measured magnetic field and ECDs of the voxels in the brain:

$$B(t) = L(\vec{r}_Q)\vec{Q}(t) \tag{14}$$

where $\vec{Q}(t)$ is ECDs in a region of interest in the brain, L is the lead field matrix, and $B(t)$ is the measured field by the sensors.

Analysis of the Model

Using the simulation results of the proposed model, we show that it is possible to detect BOLD signal in a voxel while the voxel is silent for MEG and vice versa. The model is based on equations 1 to 14 and figure 1. There are several parameters in the model, some of which are considered stochastic and others deterministic. In all simulations, the values for the deterministic and the pdfs for the stochastic parameters are as described in the previous sections (any deviation from these values will be explained).

There are approximately 10^5 neurons per mm^3 of the cortex and thousands of synapses per neuron (Hämäläinen et al. 1993). If the external stimulus causes activation in one percent of the synapses, then there are on the order of 10^6 active synapses in a voxel with a volume of 1 mm^3. The number of excitatory synapses is more than inhibitory synapses and we consider 10% for the ratio of

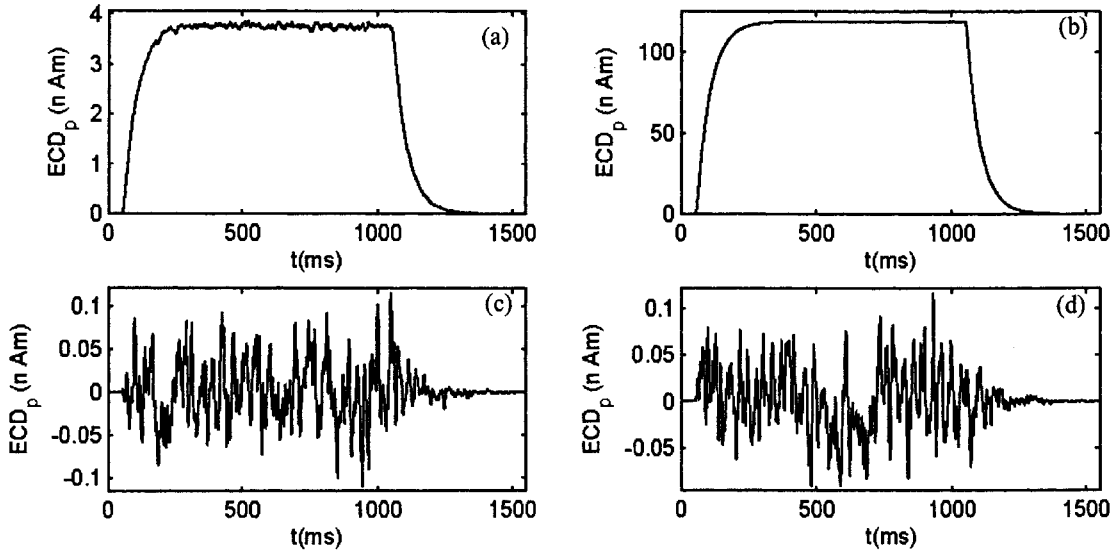

Figure 4. Illustration of cases that MEG signal is significant or small, using the effects of pdf of θ and ratio of IPSPs number to all PSPs on ECD ($Q_p(t)$) in MEG signals. (a) pdf of θ is same as figure 3b and IPSP ratio is set to 10%. (b) $f_\Theta(\theta)=\delta(\theta)$ and IPSP ratio is set to zero. (c) pdf θ is set to uniform distribution around $(-\pi, \pi)$ and IPSP ratio is set to 10%. (d) pdf θ is same as figure 3b and IPSP ratio is set to 50%.

IPSPs to all PSPs (we call this ratio as "IPSP ratio" hereafter). Figure 3 shows first simulation results in a voxel of 1 mm^3 with $N = 10^6$ active PSPs and IPSP ratio of 10%. The stimulus duration is 1 second. Number of active PSPs (sum of EPSPs and IPSPs) during stimulation is depicted in figure 3a. The current dipole produced by each PSP has an angle (θ) with the reference vector, in the $(-\pi, \pi)$ range. Figure 3b illustrates the pdf of θ for EPSPs and IPSPs.

The projected ECD to the reference vector ($Q_p(t)$) and normal to this vector ($Q_n(t)$) are depicted in figures 3c and 3d, respectively. According to equation 13 and the odd property of the sine function, the average value of $Q_n(t)$ will be zero as shown in figure 3d. It is assumed in (Hämäläinen et al. 1993) that the ECD with moment in the order of 10 nAm can be detected by the MEG sensors, although the ECDs that can be detected vary much beyond the stated 10 nAm (both upwards and downwards). Considering this detectable threshold for the moment of ECD, we find that the $Q_p(t)$ in figure 3c can be detected, although the pdf of θ tends to a uniform pdf and it is expected that PSPs cancel each other. This is according to the fact that the small difference between the pdf of θ and uniform pdf is amplified by the huge number of active PSPs and thus a detectable MEG signal is produced. Normalized synaptic activities are shown in figure 3e and are used as the input to the Balloon model. Finally, figure 3f shows the resulting BOLD signal without considering the additive noise. The maximum contrast of the BOLD signal is 1.58%.

The simulation results in figure 4 show special cases where the BOLD signal is detectable but the MEG signal may or may not be detectable. There are two parameters in the proposed model for this condition: the pdf of θ and the IPSP ratio. When the pdf of θ tends to uniform, then the directions of the current dipoles are uniformly distributed and can cancel each other. On the other hand, if the numbers of IPSP and EPSP are equal (the IPSP ratio tends to 50%) with considering the same pdf of θ for EPSP and IPSP, they cancel each other because of their opposite polarities. Since only $Q_p(t)$ correlates with the stimulation, it is illustrated in figure 4. All conditions (except for the pdf of θ and IPSP ratio) in figure 4 are the same as those in figure 3. Therefore, the BOLD output for all subplots of figure 4 will be the same as those in figure 3f (not shown to avoid repetitions) and thus there will be detectable BOLD signal in all subplots.

For a conventional condition, $Q_p(t)$ is shown in figure 4a, where the pdf of θ is the same as that in figure 3b and the IPSP ratio is set to 10%. The best condition for detecting the MEG signal is shown in figure 4b, where all current dipoles are considered parallel ($f_\Theta(\theta)=\delta(\theta)$ in equation 10) and all PSPs are considered EPSPs without any IPSP (IPSP ratio is zero). The amplitude of ECD in this condition is about 30 times larger than that of figure 4a. The pdf of θ is considered to be uniform and the IPSP ratio is set to 10% in figure 4c. In figure 4d, the IPSP ratio is set to zero and the pdf of θ is the same as that of figure

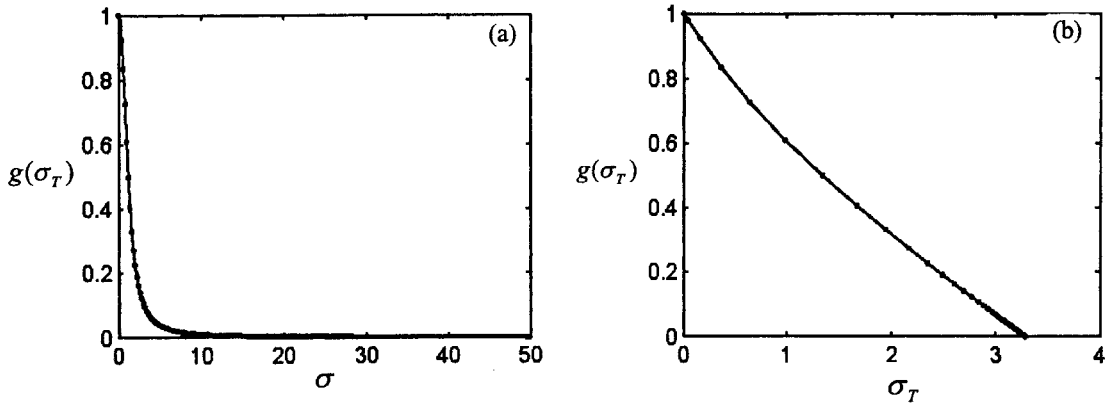

Figure 5. Illustration of the nonlinear function that relates the standard deviation of θ to ECD according to equations 18 and 21. (a) $g(\sigma_T)$ versus σ. (b) $g(\sigma_T)$ versus σ_T.

3b. The ECD in both figures 4c and 4d is like random noise with zero mean and there is no detectable MEG signal correlated with the stimulus, although there are detectable BOLD signals for both figures.

Now, we intend to quantitatively survey the effects of pdf of θ and IPSP ratio on MEG and fMRI signals. Once the number of active synapses reaches its final steady state value according to equation 1, it becomes almost constant. Referring to equation 13, we have:

$$\vec{Q}=\left[\sum_{d=0}^{D}\sum_{k=1}^{N} w_k\beta_k\Delta V_k\varphi_k(d)\cos(\theta_k)\right]\cdot\vec{n}_p+\left[\sum_{d=0}^{D}\sum_{k=1}^{N} w_k\beta_k\Delta V_k\varphi_k(d)\sin(\theta_k)\right]\cdot\vec{n}_n \tag{15}$$

where N is the average number of active synapses after steady state. If all random variables in equation 15 are considered independent, the mean value of ECD is:

$$\overline{\vec{Q}}=\left\{\sum_{d=0}^{D}\sum_{k=1}^{N} E[w_k]E[\beta_k]E[\Delta V_k]E[\varphi_k(d)]E[\cos(\theta_k)]\right\}\cdot\vec{n}_p=\overline{Q}\cdot\vec{n}_p \tag{16}$$

$$\overline{Q}=\overline{\varphi}\,\overline{V}\,\overline{\beta}\,N\left[(1-r)\,g\left(\sigma_T^E\right)-r\,g\left(\sigma_T^I\right)\right] \tag{17}$$

where $E[.]$ is "expected value", r is the mean value of IPSP ratio, $\overline{V}$ is mean amplitude of PSP, $\overline{\beta}$ is mean of β according to equation 9, $\overline{\varphi}=\sum_{d=0}^{D}E[\varphi_k(d)]$ according to $\varphi(t)$ in equation 3 with τ_{PSP} ~TN(2,1;0,∞)ms and $g\left(\sigma_T^E\right)$ and $g\left(\sigma_T^I\right)$ show average effects of the projected ECD onto the reference vector for EPSP and IPSP, respectively. The second term of equation 15 vanishes in averaging because of the odd property of the sine function and even property of the pdf of θ.

The function $g(\sigma_T)$ is the expected value of cos(θ) with respect to the truncated θ and is defined by:

$$\begin{cases} g(\sigma_T)=\int_{-\pi}^{\pi}\cos(\theta)f_\Theta(\theta)d\theta=\int_{-\pi}^{\pi}\cos(\theta)\dfrac{e^{\frac{-\theta^2}{2\sigma^2}}}{\sqrt{2\pi}\,\sigma\,erf\left(\dfrac{\pi}{\sqrt{2}\sigma}\right)}d\theta \\ \sigma_T^2=\sigma^2\left(1-\dfrac{2\pi\sigma^2}{k}e^{\frac{-\pi^2}{2\sigma^2}}\right) \end{cases} \tag{18}$$

where $f_\Theta(\theta)$ is the truncated Gaussian distribution defined in equation 10. The $g(\sigma_T)$ versus σ and σ_T is plotted in figure 5. When $\sigma\to 0$, then $\sigma_T\to 0$ and the pdf of θ tends to the Dirac delta function and $g(\sigma_T)\to 1$. When $\sigma\to\infty$, then $\sigma_T\to\pi^2/3$ and the pdf of θ tends to the uniform distribution and $g(\sigma_T)\to 0$.

According to the relationship between the synaptic activities as the input of extended Balloon model and the PSPs in equation 7, we have:

$$\begin{cases} \overline{u}\propto E\left[\sum_{k=1}^{N}\tau_{PSP}^k\Delta V_k\right] \\ \overline{u}\propto N\overline{\tau}_{PSP}\overline{V}\,k_{pyramidal}\Rightarrow\overline{u}=u_m\dfrac{N}{\max(N)} \end{cases} \tag{19}$$

where u_m is the synaptic activity that produces the satu-

rated maximum output in the extended Balloon model and max(N) shows the maximum number of PSPs in a voxel that can be activated by an external stimulus. In equation 19, N represents the number of active pyramidal cells and $k_{pyramidal}$ shows the effects of non-pyramidal cells (which is silent for MEG) on the synaptic activity, which is a constant for each voxel according to the assumptions of the Integrated Model - Construction BOLD from PSPs section. Inserting equation 19 in equation 17, we get:

$$\begin{cases} \overline{Q} = \overline{\varphi}\,\overline{V\beta}\max(N)\left[(1-r)\,g\left(\sigma_T^E\right) - r\,g\left(\sigma_T^1\right)\right]\dfrac{\overline{u}}{u_m} \\ \overline{Q} = \overline{Q}_m\left[(1-r)\,g\left(\sigma_T^E\right) - r\,g\left(\sigma_T^I\right)\right]\dfrac{\overline{u}}{\overline{u}_m} \end{cases} \quad (20)$$

Then, the relationship between BOLD and ECD is derived as:

$$\begin{cases} \overline{Q} = \overline{Q}_m\left[(1-r)\,g\left(\sigma_T^E\right) - r\,g\left(\sigma_T^I\right)\right]\dfrac{\overline{u}}{u_m} \\ BOLD\ Output = Balloon\ Model\left(\overline{u}\right) \end{cases} \quad (21)$$

According to equation 21, the nonlinear relationship between ECD and BOLD segregates into two parts: a linear relation between ECD and $\overline{u}$ (mean synaptic activity) and a nonlinear relation between BOLD and $\overline{u}$ as a result of the nonlinearity of the Balloon model.

Equation 17 shows different spatial distributions for EPSPs and IPSPs that can be modeled with different pdf of θ (different values of $g\left(\sigma_\theta^E\right)$ and $g\left(\sigma_\theta^I\right)$). In figures 6-7, our intention is to separately illustrate the effects of IPSP ratio and pdf of θ on the relationship between fMRI and MEG. In figures 6c, 7b, and 7d, our focus is illustration of the effect of IPSP ratio (r). Thus, we consider the same pdf of θ for EPSPs and IPSPs in these figures ($\sigma^E=\sigma^I=0$). This allows illustration of the effect of IPSP ratio without the effect of the pdf of θ. On the other hand, in figures 6b, 7a, and 7c, the goal is to illustrate the effect of the pdf of θ. Therefore, we consider r=0 in these figures to merely show the effect of the pdf of θ without the effect of the IPSP ratio. Note that according to equation 17 in the manuscript, when r=0 the effect of $g\left(\sigma_\theta^I\right)$ vanishes and there is no need to assume the same pdf of θ for IPSPs and EPSPs in these figures.

Figure 6a illustrates the relationship between ECD and BOLD according to equation 21 with r = 0 and $\sigma_T^E = 0\left(g\left(\sigma_T^E\right)=1\right)$ where BOLD increases and saturates as ECD increases. The curve can be separated into three regions. For increasing ECD from zero to 1%, the BOLD contrast is less than 15% of its maximum. The ECD and BOLD signals are very small and may not be detected in this region of the curve. The second part of the curve contains its steepest part where increasing ECD from 1% to 27% increases BOLD from 15% to 90%. The BOLD signal saturates in the third part where 73% increase in ECD increases BOLD signal by only 10%.

The effect of the pdf of θ on the relationship between the ECD and BOLD signals is shown in figure 6b. Three curves are plotted for $\sigma_T^E = 0, 10$ and 25 ($r = 0$ for all curves). According to figure 6b, for a large value of σ_T^E=25 (where the pdf of θ tends to uniform) when the BOLD signal is at its maximum, the ECD is less than 0.2% of its maximum and is not detectable. The effect of the IPSP ratio (r) on the relationship between the ECD and BOLD is shown in figure 6-c for three values of IPSP ratio, r = 0, 20%, and 40% ($\sigma_T^E = \sigma_T^I = 0$ for all curves). When r tends to 50% (canceling EPSPs with IPSPs), the ECD tends to zero although the BOLD signal is detectable at its maximum value.

In figure 7, a detectable signal for either ECD or BOLD is assumed and effects of σ (pdf of θ) and r (IPSP ratio) on the detection of the other one are evaluated. The contrast of BOLD is fixed at 2% in figures 7a and 7b and the resulting ECD is plotted as functions of σ and r, respectively. Note that increasing σ or r decreases ECD to zero and thus even though the BOLD signal is detectable, there may be no detectable MEG signal. In figures 7c and 7d, the value of ECD is set to a detectable level (10% of its maximum) and the resulting BOLD is plotted as functions of σ and r. Note that even with this small value of ECD, increasing σ or r increases the BOLD to its maximum.

As mentioned previously, the IPSP ratio in order of 10% is physiologically feasible in most of the cortical areas. We are not sure if the IPSP ratio of 50% is physiologically feasible. However, it is merely used to illustrate the effect of canceling the EPSPs by IPSPs in our model.

Discussion

In this paper, an integrated model for the MEG and fMRI is proposed. The PSPs are the common link between the MEG and fMRI. The parameters of the PSPs in each neuron and even in each synapse in a neuron are different. We treat each parameter of PSP as a random variable. Considering expected values of these parameters, the main relationship between ECD (in MEG) and BOLD are derived in equation 21. Two parameters exist in equation 21: the ratio of the number of active IPSPs to the number of active EPSPs and the distribution of the PSP directions. The first parameter summarizes different aspect of EPSP and IPSP for MEG and fMRI. The second one can show situations like the following. Spherically symmetric distribution of PSPs' direction can represent activities of the non-pyramidal cells or activations of the inhibitory synapses belonging to the basal dendritic tree. The sharp distribution of PSPs' direction can model the apical dendrites of the pyramidal cells for EPSPs.

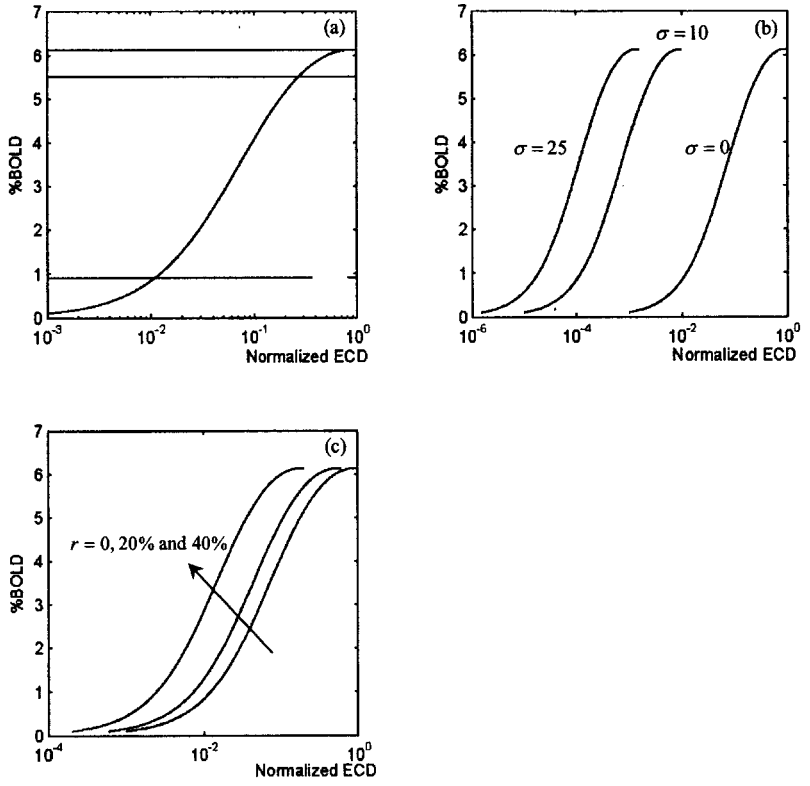

Figure 6. Illustration of the effects of two parameters (standard deviation of θ and ratio of IPSP to all PSP) on the MEG and fMRI signals. Relationship between ECD and BOLD according to equation 21 for: (a) $r = 0$ and $\sigma^E = 0\left(g\left(\sigma_T^E\right) = 1\right)$. The horizontal lines show 15%, 90% and 100% of maximum BOLD signal. (b) $r = 0$ and $\sigma^E = 0$, 10 and 25. (c) $\sigma^E = \sigma^I = 0$ and $r = 0$, 20% and 40%.

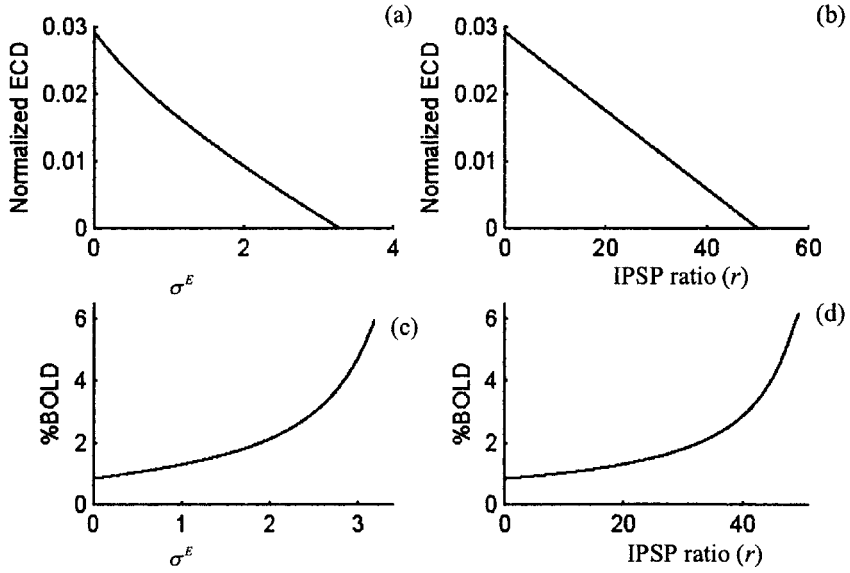

Figure 7. Illustration of the conditions where detectable fMRI signal is considered but MEG signal changes as a function of σ (pdf of θ) and r (IPSP ratio) and vice versa. (a) Contrast of BOLD is fixed at 2% and r=0. (b) Contrast of BOLD is fixed at 2% and σ^E=σ^I=0. (c) Value of ECD is fixed at 10% of its maximum value and r=0. (d) Value of ECD is fixed at 10% of its maximum value and σ^E=σ^I=0.

In the proposed model, the ratio of IPSP to EPSPs in each voxel is assumed constant during activation (as mentioned in the Integrated Model - Neural Basis of MEG and fMRI section for the effect of IPSP in fMRI). The effect of reducing the neural activities and the number of active EPSPs by shunting inhibition is considered in the model simply by the ratio of IPSP to EPSPs. If this ratio is not constant during the activation, its effect can be modeled by considering a time dependent value for this ratio.

Relationship between ECD and BOLD is nonlinear according to equation 21 and figure 6. With low neural activities, both ECD and BOLD are so weak that can not be detected. In the mid-range of the neural activity, there is almost a linear relationship between them. High neural activity saturates the BOLD while ECD may increase (figure 6a). Figure 7 illustrates situations where for a specific neural activity, it is possible to detect the BOLD signal while the ECD may or may not be detectable and vice versa.

Now, we address the synchronicity and its effect on the MEG and fMRI signals. Assume N PSPs start to fire at the same time synchronously. Peak of the measured signal by the MEG sensors is N times of that for a single PSP. Now, consider a situation in which there is no synchronicity and each PSP fire with a delay with respect to the previous PSP and the time duration from the first to the last firing is in the order of 100-200 ms (duration of PSP is in the order of 10-20 ms). In this case, the peak of the measured signal by the MEG sensors is almost equal to that of a single PSP. The delay time in the order of 100 ms has no effects on the hemodynamic response and thus the two cases are similar for the fMRI. To consider synchronicity, parameters of the linear model for relating external stimulus to the number of active synapses (block 1 of figure 1) can be changed and the number of PSPs that synchronously fire at time t can vary even with a fixed external stimulus.

There are several conditions that the MEG signal may not be produced for a given neural activity. For example, in a spherical head model, the radial dipoles and the dipole in the center of the sphere do not produce any magnetic field outside the sphere. In addition, the magnetic field which is produced by a cortical source falls off as the square of distance. Thus, superficial dipoles (that are close to the sensors) have larger contributions than the deep dipoles. Consequently, for a specific amount of neural activity and the resulting BOLD signal, the direction and location of ECD can affect the measured field by the MEG sensors. In the proposed model, the block "Lead Field from Forward Problem" and the method selected for solving the inverse problem incorporate these into the model.

Conclusion

The purpose of this paper is to present an integrated MEG and fMRI model. In the model, the neural activity is related to PSPs as the common link between MEG and fMRI. The proposed stochastic model is based on the parameters of PSPs that are considered as random variables. Neural activities in a voxel can change rCBF and produce BOLD signal in the neighboring voxels. We model this spatial blurring property of the BOLD signal as "Crosstalk from Neural Activities of Adjacent Voxels". The effects of the model's parameters are explored and illustrated using multiple simulation studies. These simulations show that the parameters of the model can explain conditions for which there is a detectable fMRI signal in a voxel but this voxel is silent for MEG and vice versa. Possible differences in the spatial responses of the MEG and fMRI can be shown using our model. The crosstalk in fMRI and ill-posedness of the inverse problem in MEG contribute to the differences in the spatial responses of the two modalities. The proposed model is instrumental in evaluating and comparing different analysis methods of MEG and fMRI. It is also useful in characterizing the upcoming methods for integrated analysis of MEG and fMRI.

References

Almeida, R. and Stetter, M. Modeling the link between functional imaging and neuronal activity: synaptic metabolic demand and spike rates. Neuroimage, 2002, 17:1065-1079.

Attwell, D. and Iadecola, C. The neural basis of functional brain imaging signals. Trends Neurosci., 2002, 25: 621-625.

Baillet, S., Mosher, J.C. and Leahy, R.M. Electromagnetic Brain Mapping. IEEE Signal Processing Magazine, 2001, 18: 14-30.

Buxhoeveden, D.P. and Casanova, M.F. The minicolumn hypothesis in neuroscience. Brain, 2002, 125: 935–951.

Buxton, R.B., Wong, E.C. and Frank, L.R. Dynamics of blood flow and oxygenation changes during brain activation: the balloon mode. Magn. Reson. Med., 1998, 39: 855-864.

Caesar, K., Gold, L. and Lauritzen, M. Context sensitivity of activity dependent increases in cerebral blood flow. Proc. Nal. Acad. Sci. USA, 2003, 100: 4239-4244.

Curio, G., Mackert, B., Burghoff, M., Koetiz, R., Abraham-Fuchs, K. and Harer, W. Localization of evoked neuromagnetic 600 Hz activity in the cerebral somatosensory system. Electroenceph. Clin. Neurophysiol., 1994, 91: 483-487.

Dale, A.M. and Halgren, E. Spatiotemporal mapping of brain activity by integration of multiple imaging modalities. Curr. Opin. Neurobiol., 2001, 11: 202-208.

Dale, A.M., Liu, A.K. and Fischl, B.R. Dynamic statistical parametric mapping: combining fMRI and MEG for high-resolution imaging of cortical activity. Neuron, 2000, 26: 55-67.

De Schutter, E. Dendritic voltage and calcium-gated channels amplify the variability of postsynaptic responses in a Purkinje cell model. J. Neurophysiol., 1998, 80: 504-519.

Friston, K.J., Mechelli, A., Turner, R. and Price, C.J. Nonlinear responses in fMRI: the balloon model, volterra kernels,

and other hemodynamics. Neuroimage, 2000, 12: 466-477.

Hämäläinen, M., Hari, R., Ilmoniemi, R.J., Knuutila, J. and Lounasmaa, O.V. Magnetoencephalography - theory, instrumentation and applications to noninvasive studies of the working human brain. Rev. of Modern Phys., 1993, 65: 413-497.

Hashimoto, I., Mashiko, T. and Imada, T. Somatic evoked high-frequency magnetic oscillations reflect activity of inhibitory interneurons in the human somatosensory cortex. Electroenceph. Clin. Neurophysiol., 1996, 100: 189-203.

Horwitz, B. and Poeppel, D. How can EEG/MEG and fMRI/PET data be combined? Human Brain Mapping, 2002, 17: 1-3.

Iadecola, C., Li, J., Xu, S. and Yang, G. Neural mechanisms of blood flow regulation during synaptic activity in cerebellar cortex. J. Neurophysiol., 1996, 75: 940-950.

Iadecola, C., Yang, G., Ebner, T.J. and Chen, G. Local and propagated vascular responses evoked by focal synaptic activity in cerebellar cortex. J. Neurophysiol., 1997, 78: 651-659.

Korvenoja, A., Aronen, H.J. and Ilmoniemi, R.J. Functional MRI as a constraint in multi-dipole models of MEG data. Int. Jour. Bioelec., 2001, Vol. 3.

Larkum, M.E., Launey, T., Dityatev, A. and Luscher, H.R. Integration of excitatory postsynaptic potentials in dendrites of motoneurons of rat spinal cord slice cultures. J. Neurophysiol., 1998, 80: 924-935.

Lauritzen, M. and Gold, L. Brain function and neurophysiological correlates of signals used in functional neuroimaging. Jour. Neurosci., 2003, 23: 3972-3980.

Liley, D.T.J. and Wright, J.J. Intracortical Connectivity of Pyramidal and Stellate Cells: Estimates of Synaptic Densities and Coupling Symmetry. Network: Computation in Neural systems, 1994.

Liu, A.K., Belliveau, J.W. and Dale, A.M. Spatiotemporal imaging of human brain activity using functional MRI constrained magnetoencephalography data: Monte-Carlo simulations. Proc. Natl. Acad. Sci. USA, 1998, 95: 8945-8950.

Logothetis, N.K. The neural basis of the blood-oxygen-level-dependent functional magnetic resonance imaging signal. Philos. Trans. R. Soc. Lond. B. Biol. Sci., 2002, 357: 1003-1037.

Logothetis, N.K. MR imaging in the non-human primate: studies of function and of dynamic connectivity. Curr. Opin. Neurobiol., 2003, 13: 630-642.

Logothetis, N.K., Pauls, J., Augath, M., Trinath, T. and Oeltermann, A. Neurophysiological investigation of the basis of the fMRI signal. Nature, 2001, 412: 150-157.

Martinez-Montes, E., Valdes-Sosa, P.A., Miwakeichi, F., Goldman, R.I. and Cohen, M.S. Concurrent EEG/fMRI analysis by multiway partial least squares. NeuroImage, 2004, 22: 1023–1034.

Nunez, P.L. and Silberstein, R.B. On the relationship of synaptic activity to macroscopic measurements: does co-registration of EEG with fMRI make sense?. Brain Topography, 2000, 13: 79–96.

Ogawa, S., Tank, D.W., Menon, R., Ellerman, J.M., Kim, S-G., Merkle, H. and Ugurbil, K. Intrinsic signal changes accompanying sensory stimulation: functional brain mapping with magnetic resonance imaging. Proc. Nat. Acad. Sci., 1992, 89: 5951-5955.

Riera, J., Aubert, E., Iwata, K., Kawashima, R., Wan, X. and Ozaki, T. Fusing EEG and fMRI based on a bottom-up model: Inferring activation and effective connectivity in neural masses. Philosophical Transactions: Biological Sciences, 2005, 360(1457): 1025-1041.

Riera, J., Bosch, J., Yamashita, O., Kawashima, R., Sadato, N., Okada, T. and Ozakic, T. fMRI activation maps based on the NN-ARx model. NeuroImage, 2004, 23: 680-697.

Tagamets, M.A. and Horwitz, B. Interpreting PET and fMRI measures of functional neural activity: the effects of synaptic inhibition on cortical activation in human imaging studies. Brain Research Bulletin, 2001, 54(3): 267-273.

Waldvogel, D., van Gelderen, P., Muellbacher, W., Ziemann, U., Immisch, I. and Hallett, M. The relative metabolic demand of inhibition and excitation. Nature, 2000, 406: 995-998.